ARTICLE

Importance of Controlling Nanotube Density for Highly Sensitive and Reliable Biosensors Functional in Physiological Conditions

Fumiaki N. Ishikawa,[†] Marco Curreli,[‡] C. Anders Olson,[‡] Hsiang-I Liao,[⊥] Ren Sun,[⊥] Richard W. Roberts,[‡] Richard J. Cote,[‡] Mark E. Thompson,[§] and Chongwu Zhou[†,*]

Departments of [†]Electrical Engineering, [‡]Chemistry, and [§]Pathology, University of Southern California, Los Angeles, California 90089, United States and [⊥]Department of Molecular and Medical Pharmacology, University of California, Los Angeles, California 90095, United States

ABSTRACT Biosensors utilizing carbon nanotube field-effect transistors have a tremendous potential to serve as the basis for the next generation of diagnostic systems. While nanotubes have been employed in the fabrication of multiple sensors, little attention has previously been paid to how the nanotube density affects the biosensor performance. We conducted a systematic study of the effect of density on the performance of nanotube biosensors and discovered that this parameter is crucial to achieving consistently high performance. We found that devices with lower density offer higher sensitivity in terms of both detection limit and magnitude of response. The low density nanotube devices resulted in a detection limit of 1 pM in an electrolyte buffer containing high levels of electrolytes (ionic concentration ~140 mM, matching the ionic strength of serum and plasma). Further investigation suggested that the enhanced sensitivity arises from the semiconductor-like behavior—strong gate dependence and lower capacitance—of the nanotube network at low density. Finally, we used the density-optimized nanotube biosensors to detect the nucleocapsid (N) protein of the SARS virus and demonstrated improved detection limits under physiological conditions. Our results show that it is critical to carefully tune the nanotube density in order to fabricate sensitive and reliable devices.

KEYWORDS: nanotube density · percolation theory · biosensing · nanotube biosensor

Single-walled carbon nanotubes (CNTs) possess a number of unique and promising properties, such as mechanical stiffness,[1,2] high carrier mobility,[3] and thermal conductivity.[4,5] Due to these properties, numerous efforts have been devoted to commercialize applications that incorporate CNTs. These applications include the next generation of transistors/circuits,[6−13] scanning probes,[14,15] mechanical composites,[16−18] and transparent electronics.[19−25] Chemical and biological sensing is one of the applications where CNTs, especially single-walled CNTs, are considered to be the ultimate type of sensors. For example, single-walled CNTs have the smallest diameters among various one-dimensional structured materials, where every atom in the CNTs is in contact with the environment.[26−44]

In the view of commercialization, researchers have traditionally preferred multiple nanotube channels in a field-effect transistor (FET) configuration (Figure 1a) over single nanotube transistors because the former offers several advantages, including higher uniformity, lower noise, and higher reproducibility.[36] While the use of such networked nanotubes as FET channels was discussed in a number of previous reports,[27,29,31−36,38,40−42] there is unfortunately minimal investigation correlating the role of the nanotube density to the biosensor performance. Several theoretical and experimental studies have proved that the density of nanotubes in the FET channel plays an important role in transistor performance.[45−48] This correlation strongly suggests that the density of nanotubes will also affect the performance of biosensors based on nanotube networks since it is likely that the sensitivity to gate modulation (FET performance) reflects the sensitivity to gating by charged captured analytes (biosensor performance), as we have shown for In_2O_3 nanowire biosensors.[49] Understanding the role of the nanotube density will lead to better designs of nanotube biosensors and more reliable fabrication procedures, both of which are extremely important.

In this context, we report our studies on the role played by the nanotube density in FET biosensor performance and demonstrate that the control of nanotube density is critical in achieving high/reliable performance (*e.g.*, high sensitivity, uniformity, re-

*Address correspondence to chongwuz@usc.edu.

Received for review May 28, 2010 and accepted October 5, 2010.

Published online October 28, 2010. 10.1021/nn101198u

producibility, *etc.*). As a first step in the study, we fabricated devices with different nanotube densities and then compared the biosensor performance of those devices. We found that the low density nanotube devices offer the best performance in terms of the magnitude of response and detection limit. Transistor measurements revealed the semiconductor-like behavior of the low density network and the quasi-metallic behavior of the high density network. Two aspects of the semiconductor-like nature were attributed to the enhanced sensitivity at low nanotube densities. First, the off-current is smaller or negligible. Second, the threshold voltage shift is enhanced due to a smaller capacitance. The latter was confirmed experimentally where we observed larger V_t shift for lower density samples. We note that this is the first observation of density-dependent V_t shift, which has never been previously discussed. Lastly, using these density-optimized devices, we detected the nucleocapsid (N) protein, a biomarker associated with the SARS coronavirus, under physiological conditions.

RESULTS AND DISCUSSION

In order to investigate the effect of the density of nanotube on the biosensor performance, we fabricated devices with different nanotube densities. The density was controlled by varying the time (10, 20, and 60 min) of incubation in the ferritin solution, which determines the density of iron-based catalyst nanoparticles on the substrate. Fabrication and experimental procedures are described in detail in the Methods section and Supporting Information. The density of nanotubes can be classified as follows: low (10 min), medium (20 min), and high (60 min) density. Typical SEM images of each density are shown in Figure 1b−d. While we have carefully maintained identical nanotube growth conditions for the three substrates, the nanotubes in the low density sample appear to be slightly shorter than the nanotubes in the medium density substrate. This variation in the length may also affect the percolation level and thus influence the electrical characteristics of the resulting FETs. We are confident that the observed differences in device performance (see below) are mainly due to different nanotube densities in the FET channel, rather than the presence of shorter nanotubes.

We first characterized the devices as transistors because the density of nanotubes has been shown to affect the transistor performance significantly,[45−49] and it is likely to reflect the sensitivity of the devices as a biosensor, as well.[48] Shown in Figure 2a−c are the typical plots of family of source−drain current (I_{ds}) *versus* source−drain voltage (V_{ds}) under different drain-back gate voltage (V_g) for each nanotube density. The step of V_g is 3 V. The device with low nanotube density (Figure 2a) exhibits clear separation along each curve, indicating stronger gate dependence for lower density nanotube devices. As the density increases from low to

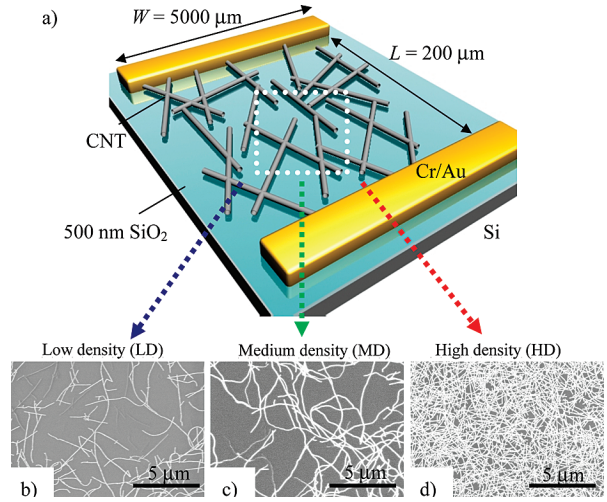

Figure 1. (a) Schematic diagram of the device structure. Typical SEM images of (b) low density, (c) medium density, and (d) high density nanotube samples.

medium to high (Figure 2b,c), the curve separation becomes less clear, indicating more metallic behavior. The linear behavior of the $I_{ds}-V_{ds}$ curves under small negative bias shows that the transport is diffusive, and the contact/junction resistance contributes little to the overall device resistance. This low contact resistance can be attributed to our devices' long channel length (~200 μm). Figure 2d shows, in log scale, the typical plots of I_{ds} *versus* V_g for low (blue), medium (green), and high (red) density nanotube devices at V_{ds} = 1 V. The low density device exhibited high on/off ratios (~10^4), while the medium density device exhibited moderate on/off ratios ($10^{1\sim2}$) and high density device exhibited low on/off ratios (<10). That correlation can be explained by the conventional percolation theory applied to carbon nanotube networks.[26,50] Figure 2e shows the same $I_{ds}-V_g$ plots in linear scale. The dashed lines in Figure 2e are the fitting curves to extract transconductance. Figure 2f shows on-current and transconductance extracted from the $I_{ds}-V_g$ curves. The saturation of transconductance was observed, while the on-current monotonically increased as the density increased. This is consistent with previous theoretical simulations and experimental observations that the capacitance of an array of aligned nanotubes saturates as the density increases because nanotubes screen each other.[10,51,52] To confirm the reproducibility of the process, we measured several devices for each density, and the distribution of on/off ratios for each density is shown in Figure 2g−i. Devices with different densities clearly exhibit different ranges of on/off ratio, confirming the reproducibility of the fabrication.

We then investigated the sensing performance of those devices using streptavidin (S-Av) as a model analyte. The sensing was carried out in 1× phosphate buffered saline (PBS). V_{ds} and drain-liquid gate voltage (V_{lg}) were 0.2 and 0 V, respectively. Constant air flow was applied to the buffer to promote mixing and minimize

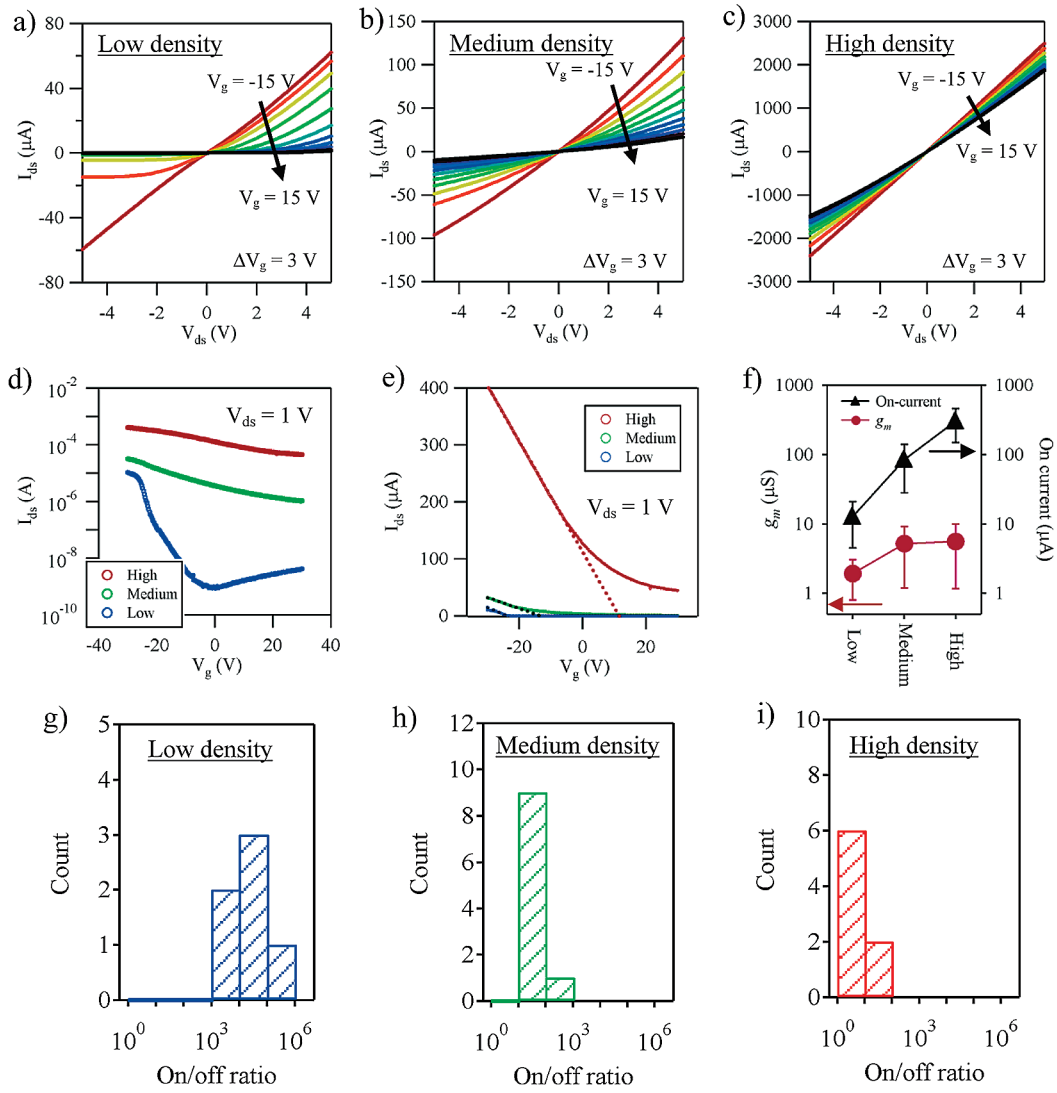

Figure 2. I_{ds} *versus* V_{ds} curves under different gate voltage ranging from −15 V (red) to 15 V (black) with a step of 3 V for (a) low density, (b) medium density, and (c) high density nanotube devices. (d) I_{ds} *versus* V_g curves at V_{ds} = 1 V in log scale for devices with each density of nanotube. (e) Curves shown in (d) plotted in linear scale. (f) On-current (left axis) and transconductance (right axis) extracted from the I_{ds} *versus* V_g curves for each density. Distribution of on/off ratio for (g) low density, (h) medium density, and (i) high density nanotube devices.

the mechanical perturbation caused by adding aliquots of buffer. The sensing experimental setup is shown in Figure S1 (Supporting Information). We note that the potential of the Pt electrode, used as a gate electrode, was stable upon exposure to streptavidin in 1× PBS, indicating little possibility for false signals as previously proposed.[53] The stability of the baseline under these conditions is discussed in the Supporting Information (Figure S2). Figure 3a shows the plot of normalized current versus time for a low density nanotube device. The device showed a ~2% decrease in conductance after exposure to 1 pM streptavidin. We attributed amine groups in streptavidin to the source of the device characteristic change since amine groups are known to have strong affinity to nanotubes with electron-donating properties and positive charges (when protonated) that are consistent with the observed trend of the changes (decrease in conductance).[26,29] The device showed further sequential decreases as the streptavidin concentration increased to 100 nM. On the other hand, when a device with the medium density nanotube was exposed to 1 and 10 pM streptavidin, there was only a negligible response (<0.5%). The device showed a change larger than 1% when the device was exposed to 100 pM streptavidin. Furthermore, the device with the high density nanotube only showed responses when exposed to 1 nM streptavidin. While the low density device clearly displayed the highest sensitivity, this device was also affected by a slightly higher noise level. We are aware that noise level can be further reduced by optimizing the device geometry (using a wider or shorter channel). For this study, we deliberately kept the device dimension constant for the three different types of devices so the nanotube density was the only variable. To summarize, Figure 3d shows plots of responses for

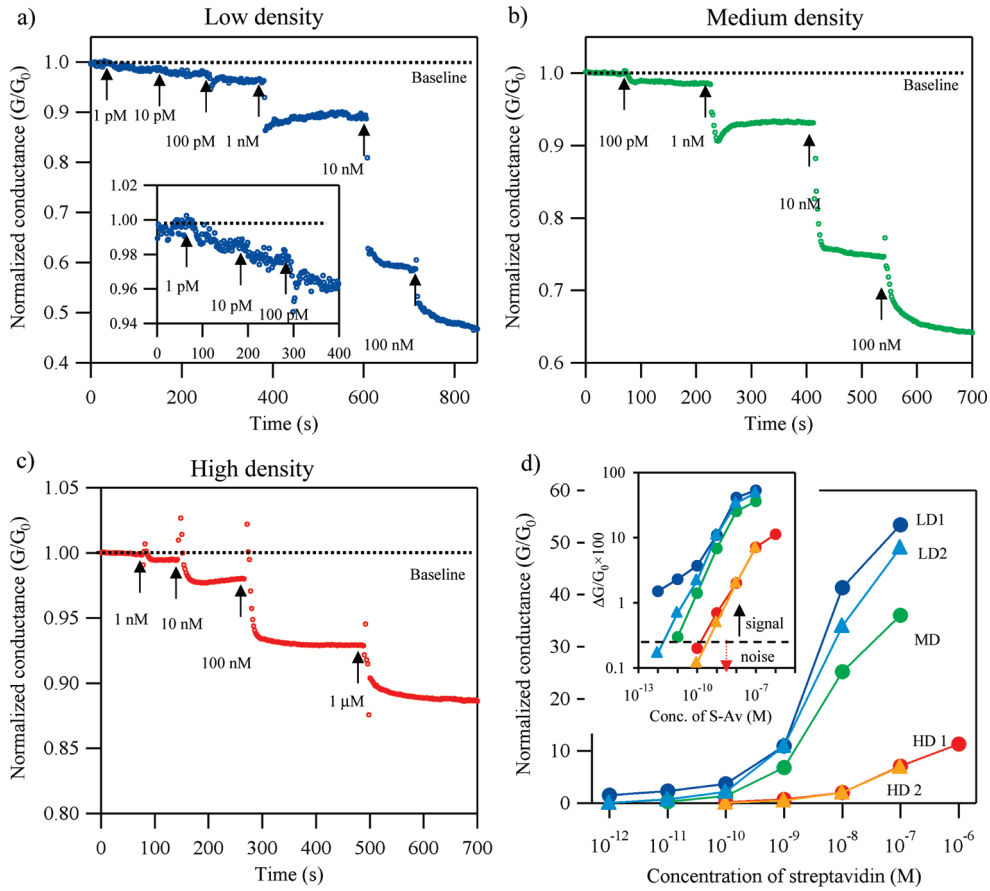

Figure 3. Plots of current *versus* time while devices were exposed to different concentrations of streptavidin for (a) low density, (b) medium density, and (c) high density nanotube devices. The experiments were carried out in 1× PBS. In these measurements, V_{ds} was 0.2 V and V_{lg} was 0 V. (d) Plots of the response signal (showed as normalized conductance) *versus* log of the concentration of streptavidin for each device with different nanotube density. The acronyms LD, MD, and HD represent low density, medium density, and high density, respectively. The inset is the same plot with the response plotted in log scale. The dashed line represents the response level of 0.5%.

each device (2 high density (HD) devices, 1 medium density (MD) device, 2 low density (LD) devices) *versus* streptavidin concentrations. The device with the low density nanotube clearly offers the highest magnitude of response to every concentration, while the device with the high density nanotube offers the lowest magnitude of response. The device with the medium density nanotube provided responses between those two extremes. The inset shows the plot of the response *versus* log of the concentration of streptavidin. In this inset, the dashed line indicated the boundary between responses with a conductance change higher than 0.5%. Changes above this line are considered true responses (signal) because the addition of buffer sometimes causes false response (noise) of ~0.2%. We did not take the thermal noise into consideration because we expect that we can reduce the thermal noise to negligible levels compared to the noise caused by the addition of the buffer by using, for example, larger channel width and lower temperature. According to this definition, the limit of detection (LOD) for high density devices falls into the 100 pM to 1 nM range, while medium density devices have an LOD of 10−100 pM. Low density devices even show an LOD of 1 pM to 10 pM, suggesting the higher sensitivity of lower density devices. These experiments clearly demonstrate the importance of the nanotube density on the biosensor performance.

This enhanced sensitivity can be partially explained by the elimination of direct metallic nanotube pathways at low density, as was confirmed in the transistor measurements (Figure 2) since conduction through metallic nanotubes is expected to be unaffected by the adsorption of proteins. However, the elimination of metallic pathways may not be the only source for this observed enhancement. In fact, the magnitude of response improved by 1 order of magnitude, while the elimination of metallic nanotube pathways is expected to improve the sensitivity only by a factor of 2−3 (from the ratio of semiconductive and metallic nanotubes). In order to investigate the source of the sensitivity enhancement, we measured the gate dependence using liquid gate before/after the sensing experiments. We exposed devices with each density to 111 nM streptavidin solution in 1× PBS, and the shift of the threshold voltage by the exposure was measured using the liquid gate. Figure 4a−c shows $I_{ds}-V_{lg}$ curves before/af-

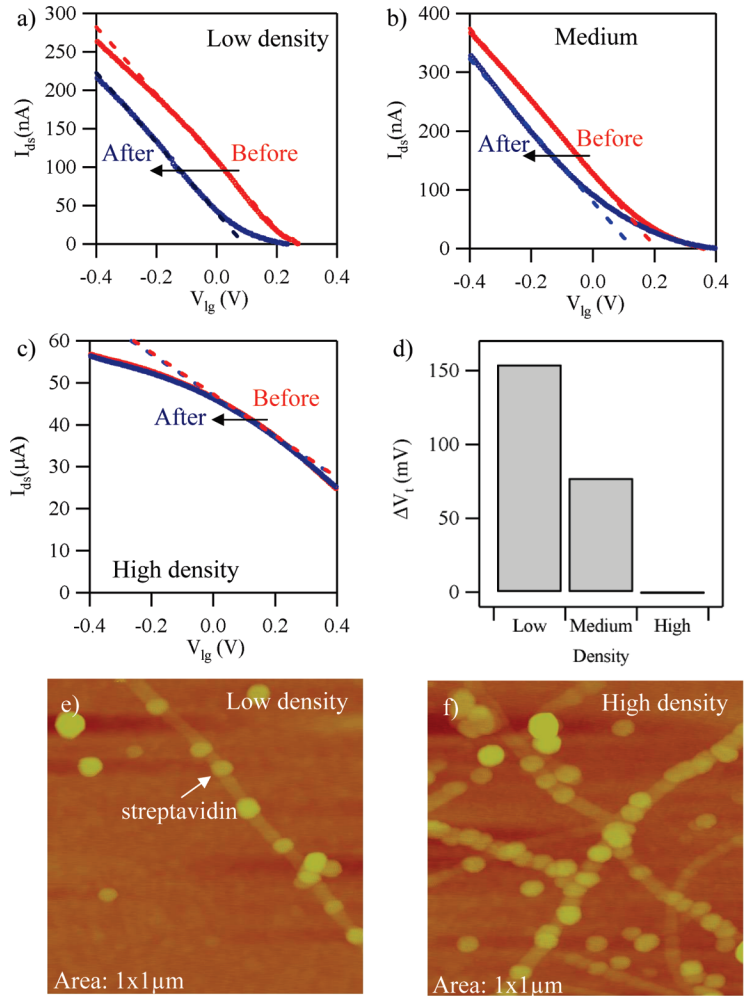

Figure 4. I_{ds} *versus* V_{lg} curves before (red) and after (blue) exposure to streptavidin at the concentration of 111 nM for (a) low density, (b) medium density, and (c) high density nanotube devices. (d) Plots of the shift of V_t for devices with each density. (e,f) AFM images of low and high density carbon nanotubes after exposure to streptavidin solution. These AFM images are obtained upon scanning an area of 1 μm × 1 μm.

ter the exposure to streptavidin for devices with each density. Figure 4d shows the plots of the V_t shift for each device. Surprisingly, the devices with lower nanotube density showed a pronounced shift in V_t compared to higher density devices, which can also contribute to the enhanced sensitivity. This is in sharp contrast to our previous observations about In_2O_3 nanowire biosensors where devices with different transistor performance showed the same amount of V_t shift after exposure to the analyte.[49] The change of the $I_{ds}-V_{lg}$ curves indicates that the sensing mechanism is due to the electrostatic interaction or charge transfer because there is little change in the transconductance. We note that in previous reports it has been proposed that the contact resistance modulation is the dominant sensing mechanism for carbon nanotube biosensors. However, this discrepancy is likely to come from the difference in the device geometry. In previous reports, a short channel length (~4 μm) was used,[54] but our devices have a long channel length (200 μm), making the channel resistance dominant in the overall device resistance. Indeed, the transistor curves show linear $I_{ds}-V_{ds}$, proving negligible contact resistance. Furthermore, a study performed by Iddo *et al.* showed that carbon nanotube biosensors can be operated by a bulk modulation mechanism with a contact passivation.[55]

We have further performed AFM imaging to estimate the number of streptavidin molecules on low and high density nanotube samples and proved that there is no significant difference in the number of streptavidin, as shown in Figure 4e,f. This suggests that the enhanced V_t shift for low density nanotubes arises from stronger interaction between nanotubes and one streptavidin molecule.

We tentatively attributed the semiconductor behavior of the low density nanotube network to the pronounced V_t shift for low density devices. When modeling the interaction between a charged protein and a nanotube as a capacitive coupling, the following relationship can be expressed:

$$\Delta Q = C_{Total} \times \Delta V$$

where ΔQ represents the amount of charges brought by the proteins, C_{Total} is the total capacitance of the carbon nanotube−double layer-liquid gate capacitor, and ΔV is the potential created by the charges on the proteins. Thus, the potential created by the charges is expressed as

$$\Delta V = \frac{\Delta Q}{C_{Total}}$$

We note that these numbers are per unit nanotube area. Total capacitance C_{Total} can be written as

$$\frac{1}{C_{Total}} = \frac{1}{C_{DL}} + \frac{1}{C_{CNT}}$$

where C_{DL} is the capacitance of the double layer and C_{CNT} is the capacitance of the carbon nanotube (quantum capacitance).[56,57] Since C_{CNT} is smaller for semiconductive nanotubes than C_{CNT} for metallic nanotubes due to the lower density of states near the Fermi level,[57] the equivalent potential ΔV becomes larger for semiconductive nanotubes. Since the characteristics of the low density nanotube network are dominated by the semiconductive nanotubes, it is likely that the low density network experiences more electrostatic interaction for a given amount of charges, that is, given amount (density) of adsorbed proteins, than the high density network which is less semiconductive.

Another possible mechanism that contributes to the density-dependent V_t shift might be the strong tube−tube screening for high density nanotube FET channels. Such screening can only be meaningful when the distance over which a charge can induce nontrivial electrostatic potential is comparable to the distance between the tube and another tube. This means the Debye length determines the area over which the tube−tube screening can play a major role. Although the Debye length of 1× PBS buffer is about 0.7 nm when calculated assuming a simple thermal equilibrium, in reality it might be significantly larger than that. Or the picture of Debye screening might not even apply to the current system, as is reported in the work by Liu *et al.*[58] According to this report, there is a shift in balance between ion diffusion and ion screening (electrostatic accumulation) to the diffusion side, due to ion flows such as electrodiffusion induced by source−drain or source−gate bias. This shift in balance leads to qualitatively different behaviors in the screening, and as a result, there is increased distance (~10 times) over which a charge can induce a nontrivial, electrostatic potential change (this might be considered as elongation of the Debye length). Under such conditions, tube−tube screening may affect the performance of nanotube biosensors by screening the charges inside an area of 10 × 10 nm^2 around tube−tube junctions. In our experiment, there might have been an external flow of ions due to the SD, SG, and DG biases. In addition, we have

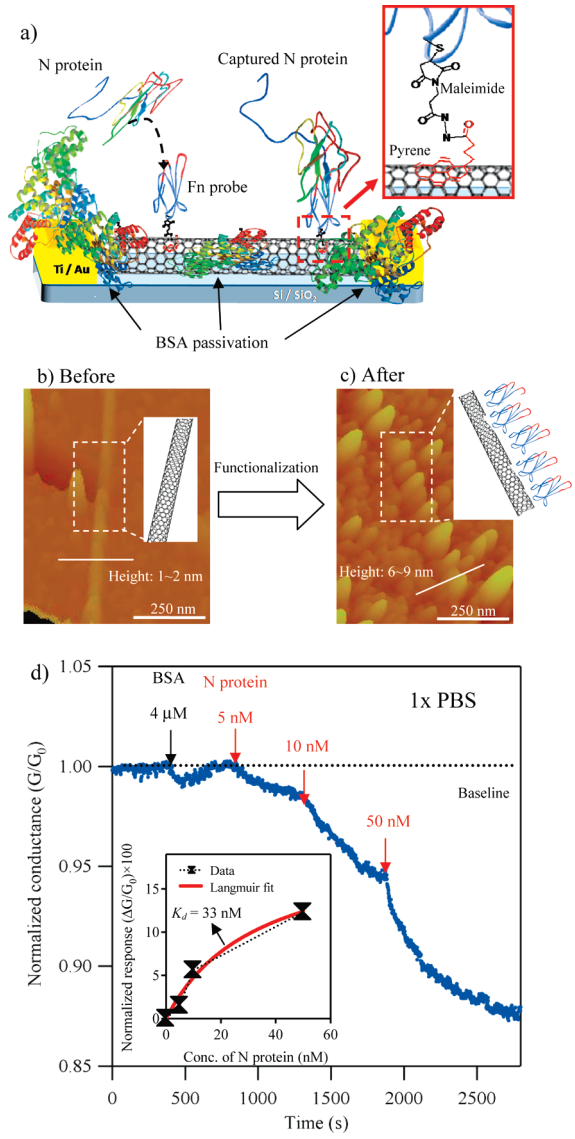

Figure 5. (a) Schematic diagram of the device structure used for N protein sensing. (b,c) AFM images of a carbon nanotube before and after the functionalization with Fn, respectively. The insets show a schematic illustration of the nanotubes. The white solid lines represent the lines along which the height profiles of the nanotube were examined. These AFM images have been resized for clarity but were originally captured upon scanning an area of 1 μm × 1 μm. (d) Plot of I_{ds} *versus* time shows the device response when sequentially exposed to 4 μM BSA and N protein at the concentrations of 5, 10, and 50 nM. The inset shows the plots of response *versus* concentration of N protein. Black marks represent the data points, and the red solid line represents a fitting using the Langmuir isotherm model.

used external air flow to enhance the mixing of the solution. This might have significantly increased the screening length of our system. We are currently investigating the effect of such external flow on biosensing.

Finally, using devices with an optimized nanotube density (low density), we successfully demonstrated the detection of the SARS biomarker protein (N protein) at physiological conditions (1× PBS) with a detection limit of 5 nM. The device preparation is shown in the Supporting Information (Figure S3). We would like

to emphasize that these detection measurements took place in a high electrolyte medium, such as 1× PBS, because we used a unique capture probe anchored to the nanotube surface. This capture probe is an engineered antibody mimic protein (AMP) based on the human fibronectin (Fn) scaffold. We have previously described the use of this AMP for nanowires biosensors.[59] Beside the high binding affinity for the target protein, this AMP is tiny in size (on the order of 3−4 nm). The captured analyte is thus held in closer contact with the nanotubes than it would be if conventional antibodies were used. Bovine serum albumin (BSA) was used to cover the empty regions of source−drain electrodes and nanotubes to prevent nonspecific binding[59] (Figure S4). The schematic diagram of the device ready for sensing is shown in Figure 5a. The AFM images of a carbon nanotube before and after functionalization with Fn are shown in Figure 5b,c, respectively. The insets in these figures show an illustration of the nanotube surface.

The selectivity of the device was first confirmed against BSA. For a density-optimized device, as shown in Figure 5d, an addition of 4 μM BSA at $t = 400$ s did not cause any stationary change in the normalized I_{ds}. On the other hand, exposing the device to N protein (5 nM) rapidly led to decreased conductance by ~2%. Further increases in the N protein concentration led to further decreases in the normalized current, confirming the selective detection of N protein. The inset of Figure 5d shows the plot of normalized response *versus* concentration of N protein with a fitting using the Langmuir isotherm model to estimate the dissociation constant (the solid red line in the inset). The fitting yielded K_d of 33 nM, while K_d estimated from surface plasmon resonance was 3 nM.[59] The discrepancy might arise from structural disorder caused by absorption of the branches of Fn onto the nanotubes. While Fn is anchored onto the nanotubes at the C-terminus to maintain the active orientation, part of Fn might be attracted to the nanotube surface due to hydrophobic interaction, thus causing a structural disorder. Clearly, the density-optimized device can be used as a detection tool to find the N protein under conditions similar to physiological fluids. This ability to operate in high electrolyte concentrations is a critical characteristic for practical applications of this technology.

In conclusion, our study has revealed the importance of considering the nanotube density when designing carbon nanotube biosensors. We have proposed that percolation and tube−tube screening play important roles in the enhanced sensitivity of low density devices. We have also shown how our newly developed biosensors can be used as a quick diagnostic tool for high-profile diseases, such as SARS. The detection of the SARS biomarker in a condition closer to the physiological conditions is a critical step toward the practical application of such nanobiosensors.

METHODS

Nanotube FET biosensors were fabricated following a previously reported method with a few modifications.[44] Briefly, nanotubes were grown by chemical vapor deposition (CVD), a method that consistently results in high-quality, low-defect, single-walled nanotubes with an average diameter of 1−2 nm and average length of 5−30 μm. The nanotube density in the FET channel was determined by controlling the deposition time of ferritin (catalyst nanoparticle precursor) on the Si/SiO_2 substrate. An aqueous solution of ferritin was obtained by diluting 1:100 the stock solution of ferritin with DI water. The Si/SiO_2 substrate was soaked in this ferritin solution for 10, 20, or 60 min. The ferritin-coated substrate was then annealed at 700 °C for 10 min to form iron-based nanoparticles to be used later as catalysts for the CVD growth of carbon nanotubes. Nanotubes were grown for 10 min at 900 °C using 2500 sccm of methane, 10 sccm of ethylene, and 600 sccm of hydrogen. Metal electrodes (10 nm Cr and 40 nm Au) were deposited through a shadow mask, which yielded devices with 200 μm channel length and 5 mm channel width, as indicated in Figure 1a. This wide area of the nanotube network makes different batches of devices have similar electrical characteristics, decreasing the device to device variation and increasing the reproducibility of results. Unwanted nanotubes located outside the channel were etched by oxygen plasma, while the channel was covered with a protecting film of poly(methyl methacrylate). The entire fabrication process leaves nanotubes intact and clean,[44] an ideal condition for the fundamental studies conducted here.

Acknowledgment. The authors acknowledge financial support from the L.K. Whittier Foundation, the National Institutes of Health, and the National Science Foundation (CCF-0726815, CCF-0702204, AI085583, and EB008275).

Supporting Information Available: Materials, experimental setup for biosensing, stability of the Pt gate potential upon exposure to streptavidin, surface functionalization of carbon nanotubes for N protein sensing, and surface saturation with BSA. This material is available free of charge *via* the Internet at http://pubs.acs.org.

REFERENCES AND NOTES

1. Yakobson, B. I.; Avouris, P. Mechanical Properties of Carbon Nanotubes. *Carbon Nanotubes* **2001**, *80*, 287.
2. Falvo, M. R.; Clary, G. J.; Taylor, R. M.; Chi, V.; Brooks, F. P.; Washburn, S.; Superfine, R. Bending and Buckling of Carbon Nanotubes under Large Strain. *Nature* **1997**, *389*, 582.
3. Durkop, T.; Getty, S. A.; Cobas, E.; Fuhrer, M. S. Extraordinary Mobility in Semiconducting Carbon Nanotubes. *Nano Lett.* **2004**, *4*, 35.
4. Hone, J.; Whitney, M.; Piskoti, C.; Zettl, A. Thermal Conductivity of Single-Walled Carbon Nanotubes. *Phys. Rev. B* **1999**, *59*, R2514.
5. Hone, J.; Whitney, M.; Zettl, A. Thermal Conductivity of Single-Walled Carbon Nanotubes. *Synth. Met.* **1999**, *103*, 2498.
6. Tans, S. J.; Verschueren, A. R. M.; Dekker, C. Room-Temperature Transistor Based on a Single Carbon Nanotube. *Nature* **1998**, *393*, 49.
7. Bachtold, A.; Hadley, P.; Nakanishi, T.; Dekker, C. Logic Circuits with Carbon Nanotube Transistors. *Science* **2001**, *294*, 1317.
8. Martel, R.; Schmidt, T.; Shea, H. R.; Hertel, T.; Avouris, P. Single- and Multi-Wall Carbon Nanotube Field-Effect Transistors. *Appl. Phys. Lett.* **1998**, *73*, 2447.

9. Chen, Z. H.; Appenzeller, J.; Lin, Y. M.; Sippel-Oakley, J.; Rinzler, A. G.; Tang, J. Y.; Wind, S. J.; Solomon, P. M.; Avouris, P. An Integrated Logic Circuit Assembled on a Single Carbon Nanotube. *Science* **2006**, *311*, 1735.
10. Kang, S. J.; Kocabas, C.; Ozel, T.; Shim, M.; Pimparkar, N.; Alam, M. A.; Rotkin, S. V.; Rogers, J. A. High-Performance Electronics Using Dense, Perfectly Aligned Arrays of Single-Walled Carbon Nanotubes. *Nat. Nanotechnol.* **2007**, *2*, 230.
11. Javey, A.; Kim, H.; Brink, M.; Wang, Q.; Ural, A.; Guo, J.; McIntyre, P.; McEuen, P.; Lundstrom, M.; Dai, H. J. High-Kappa Dielectrics for Advanced Carbon-Nanotube Transistors and Logic Gates. *Nat. Mater.* **2002**, *1*, 241.
12. Cao, Q.; Kim, H. S.; Pimparkar, N.; Kulkarni, J. P.; Wang, C. J.; Shim, M.; Roy, K.; Alam, M. A.; Rogers, J. A. Medium-Scale Carbon Nanotube Thin-Film Integrated Circuits on Flexible Plastic Substrates. *Nature* **2008**, *454*, 495.
13. Ryu, K.; Badmaev, A.; Wang, C.; Lin, A.; Patil, N.; Gomez, L.; Kumar, A.; Mitra, S.; Wong, H. S. P.; Zhou, C. W. CMOS-Analogous Wafer-Scale Nanotube-on-Insulator Approach for Submicrometer Devices and Integrated Circuits Using Aligned Nanotubes. *Nano Lett.* **2009**, *9*, 189.
14. Dai, H. J.; Hafner, J. H.; Rinzler, A. G.; Colbert, D. T.; Smalley, R. E. Nanotubes as Nanoprobes in Scanning Probe Microscopy. *Nature* **1996**, *384*, 147.
15. Wong, S. S.; Joselevich, E.; Woolley, A. T.; Cheung, C. L.; Lieber, C. M. Covalently Functionalized Nanotubes as Nanometre-Sized Probes in Chemistry and Biology. *Nature* **1998**, *394*, 52.
16. Schadler, L. S.; Giannaris, S. C.; Ajayan, P. M. Load Transfer in Carbon Nanotube Epoxy Composites. *Appl. Phys. Lett.* **1998**, *73*, 3842.
17. Kuzumaki, T.; Miyazawa, K.; Ichinose, H.; Ito, K. Processing of Carbon Nanotube Reinforced Aluminum Composite. *J. Mater. Res.* **1998**, *13*, 2445.
18. Shaffer, M. S. P.; Windle, A. H. Fabrication and Characterization of Carbon Nanotube/Poly(vinyl alcohol) Composites. *Adv. Mater.* **1999**, *11*, 937.
19. Cao, Q.; Hur, S. H.; Zhu, Z. T.; Sun, Y. G.; Wang, C. J.; Meitl, M. A.; Shim, M.; Rogers, J. A. Highly Bendable, Transparent Thin-Film Transistors That Use Carbon-Nanotube-Based Conductors and Semiconductors with Elastomeric Dielectrics. *Adv. Mater.* **2006**, *18*, 304.
20. Cao, Q.; Zhu, Z. T.; Lemaitre, M. G.; Xia, M. G.; Shim, M.; Rogers, J. A. Transparent Flexible Organic Thin-Film Transistors That Use Printed Single-Walled Carbon Nanotube Electrodes. *Appl. Phys. Lett.* **2006**, *88*, 113511.
21. Artukovic, E.; Kaempgen, M.; Hecht, D. S.; Roth, S.; GrUner, G. Transparent and Flexible Carbon Nanotube Transistors. *Nano Lett.* **2005**, *5*, 757.
22. Ishikawa, F. N.; Chang, H. K.; Ryu, K.; Chen, P. C.; Badmaev, A.; De Arco, L. G.; Shen, G. Z.; Zhou, C. W. Transparent Electronics Based on Transfer Printed Aligned Carbon Nanotubes on Rigid and Flexible Substrates. *ACS Nano* **2009**, *3*, 73.
23. Zhang, D. H.; Ryu, K.; Liu, X. L.; Polikarpov, E.; Ly, J.; Tompson, M. E.; Zhou, C. W. Transparent, Conductive, and Flexible Carbon Nanotube Films and Their Application in Organic Light-Emitting Diodes. *Nano Lett.* **2006**, *6*, 1880.
24. Wu, Z. C.; Chen, Z. H.; Du, X.; Logan, J. M.; Sippel, J.; Nikolou, M.; Kamaras, K.; Reynolds, J. R.; Tanner, D. B.; Hebard, A. F.; *et al.* Transparent, Conductive Carbon Nanotube Films. *Science* **2004**, *305*, 1273.
25. Neff, P. A.; Wunderlich, B. K.; Lud, S. Q.; Bausch, A. R. Silicon-on-Insulator Based Thin Film Resistors for Quantitative Biosensing Applications. *Phys. Status Solidi A* **2006**, *203*, 3417.
26. Kong, J.; Franklin, N. R.; Zhou, C. W.; Chapline, M. G.; Peng, S.; Cho, K. J.; Dai, H. J. Nanotube Molecular Wires as Chemical Sensors. *Science* **2000**, *287*, 622.
27. Chen, R. J.; Bangsaruntip, S.; Drouvalakis, K. A.; Kam, N. W. S.; Shim, M.; Li, Y. M.; Kim, W.; Utz, P. J.; Dai, H. J. Noncovalent Functionalization of Carbon Nanotubes for Highly Specific Electronic Biosensors. *Proc. Natl. Acad. Sci. U.S.A.* **2003**, *100*, 4984.
28. Besteman, K.; Lee, J. O.; Wiertz, F. G. M.; Heering, H. A.; Dekker, C. Enzyme-Coated Carbon Nanotubes as Single-Molecule Biosensors. *Nano Lett.* **2003**, *3*, 727.
29. Star, A.; Gabriel, J. C. P.; Bradley, K.; Gruner, G. Electronic Detection of Specific Protein Binding Using Nanotube FET Devices. *Nano Lett.* **2003**, *3*, 459.
30. So, H. M.; Won, K.; Kim, Y. H.; Kim, B. K.; Ryu, B. H.; Na, P. S.; Kim, H.; Lee, J. O. Single-Walled Carbon Nanotube Biosensors Using Aptamers as Molecular Recognition Elements. *J. Am. Chem. Soc.* **2005**, *127*, 11906.
31. Panchapakesan, B.; Cesarone, G.; Teker, K.; Wickstrom, E. Single Wall Carbon Nanotubes with Adsorbed Monoclonal Antibodies Detect Breast Cancer Cells. *Clin. Cancer Res.* **2005**, *11*, 9064S.
32. Li, C.; Curreli, M.; Lin, H.; Lei, B.; Ishikawa, F. N.; Datar, R.; Cote, R. J.; Thompson, M. E.; Zhou, C. W. Complementary Detection of Prostate-Specific Antigen Using In_2O_3 Nanowires and Carbon Nanotubes. *J. Am. Chem. Soc.* **2005**, *127*, 12484.
33. Byon, H. R.; Choi, H. C. Network Single-Walled Carbon Nanotube-Field Effect Transistors (SWNT-FETs) with Increased Schottky Contact Area for Highly Sensitive Biosensor Applications. *J. Am. Chem. Soc.* **2006**, *128*, 2188.
34. Star, A.; Tu, E.; Niemann, J.; Gabriel, J. C. P.; Joiner, C. S.; Valcke, C. Label-Free Detection of DNA Hybridization Using Carbon Nanotube Network Field-Effect Transistors. *Proc. Natl. Acad. Sci. U.S.A.* **2006**, *103*, 921.
35. Star, A.; Joshi, V.; Skarupo, S.; Thomas, D.; Gabriel, J. C. P. Gas Sensor Array Based on Metal-Decorated Carbon Nanotubes. *J. Phys. Chem. B* **2006**, *110*, 21014.
36. Snow, E. S.; Perkins, F. K.; Robinson, J. A. Chemical Vapor Detection Using Single-Walled Carbon Nanotubes. *Chem. Soc. Rev.* **2006**, *35*, 790.
37. Gruner, G. Carbon Nanotube Transistors for Biosensing Applications. *Anal. Bioanal. Chem.* **2006**, *384*, 322.
38. Tang, X. W.; Bansaruntip, S.; Nakayama, N.; Yenilmez, E.; Chang, Y. L.; Wang, Q. Carbon Nanotube DNA Sensor and Sensing Mechanism. *Nano Lett.* **2006**, *6*, 1632.
39. Abe, M.; Murata, K.; Kojima, A.; Ifuku, Y.; Shimizu, M.; Ataka, T.; Matsumoto, K. Quantitative Detection of Protein Using a Top-Gate Carbon Nanotube Field Effect Transistor. *J. Phys. Chem. C* **2007**, *111*, 8667.
40. Gui, E. L.; Li, L. J.; Zhang, K. K.; Xu, Y. P.; Dong, X. C.; Ho, X. N.; Lee, P. S.; Kasim, J.; Shen, Z. X.; Rogers, J. A.; *et al.* DNA Sensing by Field-Effect Transistors Based on Networks of Carbon Nanotubes. *J. Am. Chem. Soc.* **2007**, *129*, 14427.
41. Shao, N.; Wickstrom, E.; Panchapakesan, B. Nanotube-Antibody Biosensor Arrays for the Detection of Circulating Breast Cancer Cells. *Nanotechnology* **2008**, *19*, 465101.
42. So, H. M.; Park, D. W.; Jeon, E. K.; Kim, Y. H.; Kim, B. S.; Lee, C. K.; Choi, S. Y.; Kim, S. C.; Chang, H.; Lee, J. O. Detection and Titer Estimation of *Escherichia coli* Using Aptamer-Functionalized Single-Walled Carbon-Nanotube Field-Effect Transistors. *Small* **2008**, *4*, 197.
43. Wang, C. W.; Pan, C. Y.; Wu, H. C.; Shih, P. Y.; Tsai, C. C.; Liao, K. T.; Lu, L. L.; Hsieh, W. H.; Chen, C. D.; Chen, Y. T. *In Situ* Detection of Chromogranin a Released from Living Neurons with a Single-Walled Carbon-Nanotube Field-Effect Transistor. *Small* **2007**, *3*, 1350.
44. Ishikawa, F. N.; Stauffer, B.; Caron, D. A.; Zhou, C. Rapid and Label-Free Cell Detection by Metal-Cluster-Decorated Carbon Nanotube Biosensors. *Biosens. Bioelectron.* **2009**, *24*, 2967.
45. Snow, E. S.; Novak, J. P.; Campbell, P. M.; Park, D. Random Networks of Carbon Nanotubes as an Electronic Material. *Appl. Phys. Lett.* **2003**, *82*, 2145.
46. Kumar, S.; Murthy, J. Y.; Alam, M. A. Percolating Conduction in Finite Nanotube Networks. *Phys. Rev. Lett.* **2005**, *95*, 66802.
47. Kumar, S.; Pimparkar, N.; Murthy, J. Y.; Alam, M. A. Theory of Transfer Characteristics of Nanotube Network Transistors. *Appl. Phys. Lett.* **2006**, *88*, 123505.

48. Kumar, S.; Blanchet, G. B.; Hybertsen, M. S.; Murthy, J. Y.; Alam, M. A. Performance of Carbon Nanotube-Dispersed Thin-Film Transistors. *Appl. Phys. Lett.* **2006**, *89*, 143501.
49. Ishikawa, F. N.; Curreli, M.; Chen, P. C.; Zhang, R.; Cote, R. J.; Thompson, M. E.; Zhou, C. A Calibration Method for Nanowire Biosensors to Suppress Device-to-Device Variation. *ACS Nano* **2009**, *3*, 3969.
50. Deng, J.; Ghosh, K.; Wong, H. S. P. Modeling Carbon Nanotube Sensors. *IEEE Sens. J.* **2007**, *7*, 1356.
51. Guo, J.; Goasguen, S.; Lundstrom, M.; Datta, S. Metal-Insulator-Semiconductor Electrostatics of Carbon Nanotubes. *Appl. Phys. Lett.* **2002**, *81*, 1486.
52. Cao, Q.; Xia, M. G.; Kocabas, C.; Shim, M.; Rogers, J. A.; Rotkin, S. V. Gate Capacitance Coupling of Singled-Walled Carbon Nanotube Thin-Film Transistors. *Appl. Phys. Lett.* **2007**, *90*, 23516.
53. Minot, E. D.; Janssens, A. M.; Heller, I.; Heering, H. A.; Dekker, C.; Lemay, S. G. Carbon Nanotube Biosensors: The Critical Role of the Reference Electrode. *Appl. Phys. Lett.* **2007**, *91*, 93507.
54. Chen, R. J.; Choi, H. C.; Bangsaruntip, S.; Yenilmez, E.; Tang, X. W.; Wang, Q.; Chang, Y. L.; Dai, H. J. An Investigation of the Mechanisms of Electronic Sensing of Protein Adsorption on Carbon Nanotube Devices. *J. Am. Chem. Soc.* **2004**, *126*, 1563.
55. Heller, I.; Janssens, A. M.; Mannik, J.; Minot, E. D.; Lemay, S. G.; Dekker, C. Identifying the Mechanism of Biosensing with Carbon Nanotube Transistors. *Nano Lett.* **2008**, *8*, 591.
56. Rosenblatt, S.; Yaish, Y.; Park, J.; Gore, J.; Sazonova, V.; McEuen, P. L. High Performance Electrolyte Gated Carbon Nanotube Transistors. *Nano Lett.* **2002**, *2*, 869.
57. Snow, E. S.; Perkins, F. K. Capacitance and Conductance of Single-Walled Carbon Nanotubes in the Presence of Chemical Vapors. *Nano Lett.* **2005**, *5*, 2414.
58. Liu, Y.; Sauer, J.; Dutton, R. W. Effect of Electrodiffusion Current Flow on Electrostatic Screening in Aqueous Pores. *J. Appl. Phys.* **2008**, *103*, 84701.
59. Ishikawa, F. N.; Chang, H.-K.; Curreli, M.; Hsiang-I Liao; Olson, C. A.; Chen, P.-C.; Zhang, R.; Roberts, R. W.; Sun, R.; Cote, R. J.; *et al.* Label-Free, Electrical Detection of the SARS Virus N-Protein with Nanowire Biosensors Utilizing Antibody Mimics as Capture Probes. *ACS Nano* **2009**, *3*, 1219.